Applied Surface Science 617 (2023) 156519

Contents lists available at ScienceDirect

Applied Surface Science

journal homepage: www.elsevier.com/locate/apsusc

Full Length Article

Multifunctional silver-coated transparent TiO_2 thin films for photocatalytic and antimicrobial applications

J.G. Cuadra [a,*], S. Molina-Prados [b], Gladys Mínguez-Vega [b], Ana.C. Estrada [c], T. Trindade [c], C. Oliveira [d], M.P. Seabra [e], J. Labrincha [e], S. Porcar [a], R. Cadena [a], D. Fraga [a], J.B. Carda [a]

[a] Department of Inorganic and Organic Chemistry, Universitat Jaume I, Avda. Sos Baynat s/n, 12071 Castellon, Spain
[b] GROC-UJI, Institute of New Imaging Technologies, Universitat Jaume I, Avda. Sos Baynat s/n, 12071 Castellon, Spain
[c] Department of Chemistry, CICECO-Aveiro Institute of Materials, University of Aveiro, 3810-193 Aveiro, Portugal
[d] Department of Biology, CESAM, University of Aveiro, Campus Universitário de Santiago, 3810-193 Aveiro, Portugal
[e] Materials and Ceramic Engineering Department, CICECO, University of Aveiro, Campus Universitário de Santiago, 3810-193 Aveiro, Portugal

ARTICLE INFO

Keywords:
Transparent thin films
Spray pyrolysis
Laser ablation
Antimicrobial activity
Photocatalysis

ABSTRACT

Transparent TiO_2 thin films coated with Ag NPs were synthesized using two industrially applicable techniques, pulsed laser ablation (PLAL) and spray pyrolysis without using high vacuum. These transparent thin films were deposited on glass in order to generate glass materials with photocatalytic and antimicrobial properties and a minimum loss of transparency. The structural, morphological and optical properties of the thin films were examined using Grazing incidence X-ray diffraction (GIXRD), Raman spectroscopy, Scanning electron microscopy (SEM) and ultraviolet–visible spectroscopy. Transmission electron microscopy (TEM) was used to identify the NPs on the TiO_2 surface. The transmittance value for the thin films was greater than 80%.The thin films thus synthesized were then assessed to determine their photocatalytic capacity by monitoring the degradation of Rhodamine B (RhB) under UV light irradiation. Ag NPs on the TiO_2 surface ensures an improvement in the photocatalytic properties, with a 99% degradation of RhB in 210 min under UV light. In addition, these transparent thin films showed high antimicrobial activity on Gram-negative bacteria when irradiated by UV light for 4 h, killing 93% of these bacteria.

1. Introduction

Over the past few years, the interest in thin film technology has grown greatly due to its wide range of applications such as photovoltaic solar cells [1], gas sensors [2], energy storage [3], heterogeneous photocatalysis for water splitting processes [4] or antimicrobial action [5]. In addition, as a consequence of the COVID-19 pandemic, the development of antivirus and antimicrobial materials has become increasingly relevant all over the world. Accordingly, the possibility of being able to functionalize diverse types of surfaces without changing their optical properties has become a priority. There are many methods to obtain thin films including electroplating [6], anodic treatment [7], chemical vapor deposition (CVD) [8], atomic layer deposition (ALD), or spin coating [9]. All of them are difficult to adapt to industry due to the fact that they are techniques that need a high vacuum or are technically very sophisticated. The spray pyrolysis method is the most readily applicable to industry because it offers an easy way to make films with any material in any quantity by simply adding it to the spray precursor solution. Moreover, it does not need a vacuum to be applied or eminence targets and quality substrates, which could be a fine advantage if the method is to be scaled up [10]. One of the most widely studied materials in thin films is titanium oxide (TiO_2) because it shows tunable behavior depending on the preparation method used [11]. By changing the preparation conditions, distinct structural polymorphs and different degrees of crystallinity [12] or amorphousness [13] can be obtained. When it is in its crystalline form, the crystal size take on special importance, and even more so if photocatalysis is being studied. On the other hand, the different polymorphic phases of TiO_2 (rutile, anatase) are of great importance in the application of the material. The anatase–rutile transition occurs at high temperatures (600 °C-700 °C). The absorption in the diverse phases is different, and hence the value of the band gap for anatase is 3.2–3.9 eV [14] and the value of the band gap for the rutile phase is 3.0–3.57 eV [15]. However, the anatase phase only absorbs in the ultraviolet spectrum (UV), and thus strategies to red-shift

* Corresponding authorat: Department of Inorganic and Organic Chemistry, Universitat Jaume I, Avda. Sos Baynat s/n, 12071, Castellón, Spain.
E-mail address: jcuadra@uji.es (J.G. Cuadra).

https://doi.org/10.1016/j.apsusc.2023.156519
Received 24 November 2022; Received in revised form 30 December 2022; Accepted 19 January 2023
Available online 21 January 2023

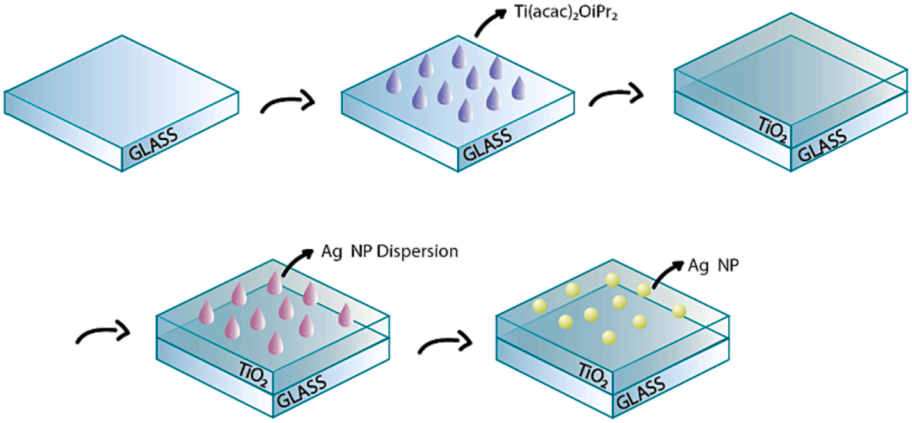

Fig. 1. Formation process of transparent TiO_2-Ag NPs thin films on soda-lime glass.

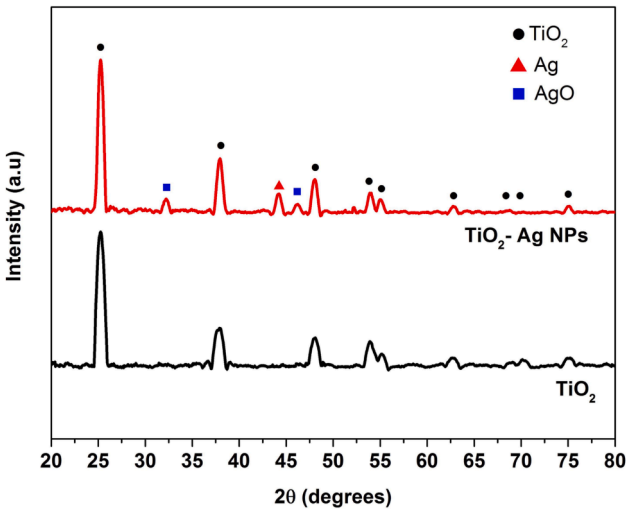

Fig. 2. GIXRD pattern of transparent TiO_2 and TiO_2-Ag NPs thin films.

the absorbance range have been explored, namely by varying the morphology of the crystals [16], introducing transition metals as dopants [17] or generating nanocomposites [18]. In this context, the binding of metal nanoparticles to semiconductors such as ZnO or TiO_2 to form Schottky Barriers due to the excellent photoelectric response it exhibited has already been reported by other authors [19,20]. Furthermore, Ag is a well-known antimicrobial agent and consequently its presence on the surface of thin films of metal oxides improves the antimicrobial activity [21]. Although there are many protocols available for nanoparticle synthesis, Pulsed Laser Ablation in Liquids (PLAL) was selected due to the simplicity of the technique [22–24]. In PLAL, the interaction of the laser radiation with a target immersed in a liquid promotes the extraction of material from the surface of the target through the formation of nanoparticles that are collected in the liquid as colloids. The technique allows synthesis of nanoparticles from a broad library of available materials and provides nanomaterials with a high degree of purity, since only the solvent and desired material are required, thereby avoiding the presence and generation of toxic or hazardous adducts and byproducts, and providing electrostatically stabilized colloids for noble metals. In the framework of the cost-effective and green development of nanotechnologies this synthesis route provides key advantages, such as as running at room temperature and ambient pressure [25] and a high production (grams per hour) compatible with industrial applications [26]. Moreover, different techniques have been adopted to adapt the beam delivery system to improve the efficiency of the process [27,28]. Additionally, to the best of the authors' knowledge the combination of these two techniques for the formation of transparent layers with nanoparticles has not been previously reported.

In this work, a facile synthesis method was used to prepare transparent TiO_2 and TiO_2-Ag NPs thin films where Ag NPs were placed on the surface of TiO_2 thin films with the aim of improving the photocatalytic and antimicrobial properties.

2. Experimental section

2.1. Materials

Titanium (IV) bis(acetylacetonate) diisopropoxide ($[(CH_3)_2CHO]_2Ti(C_5H_7O_2)_2$ 75 wt% in isopropanol, Sigma-Aldrich), ethanol (EtOH, Scharlau), Ammonia 30 % (w/w) (NH_3, PanReactAppliChem) and deionized water with pH of 6.9 ± 0.2. The dye (purchased through Fraga Lab, Mexico) used to test the photocatalytic activity of the TiO_2 was Rhodamine B (RhB), with an Mw of 479.01 g/mol, and a purity of 95 %. Milli-Q deionized water with a resistivity of 18.2 MΩ-cm (Ultramatic Plus, Wasserlab, Spain) and ultrapure silver foil (Silver, Aldrich Chemistry) were used for colloid synthesis. *tert*-butyl alcohol (*t*-BuOH), formic acid (HCOOH) and 1,4-Benzoquinone ($C_6H_4O_2$) (99 %, purity) were acquired from Sigma-Aldrich.

2.2. Methods

The crystalline structure of transparent thin films composed of TiO_2 and TiO_2-Ag NPs was studied using Grazing incidence X-ray diffraction (GIXRD) measurements. An X-ray diffractometer (D4 Endeavor, Burker-ASX) armed with a Cu K_α radiation source was used. Data were obtained by step-scanning from 20° to 80° with a step size of 0.05° 2θ and 3 s counting time per step. The measurements were accomplished at a grazing-incident angle greater than the so-called critical angle for total external reflection at which X-rays penetrate the sample. The critical angle (around 1°) was determined through testing. Scanning Electron Microscopy (SEM), performed on JEOL 7001F equipment, was engaged to study the surface, the sectional morphology and the thickness of the films. SEM-EDS mappings were recorded at an acceleration voltage of 12 kV and a moderate beam current of 0.8nA. Spectra were recorded at a step size of 0.3 μm and a low dwell time of 0.3 msec using drift correction. The software package Aztec 4.3 (Oxford Instruments, UK) was used to record the EDS analyses. The layer thickness was determined from cross-section micrographs. Transmission electron microscopy (TEM) was performed using a Hitachi H-9000 TEM microscope (Chiyoda, Tokyo, Japan) carried out at an accelerating voltage of 300 kV. The thin layer was removed with a micro-blade and then dispersed in EtOH. A drop (10 μL) of a suspension of the removed thin film dispersed in ethanol was placed on a copper grid with a lacey amorphous

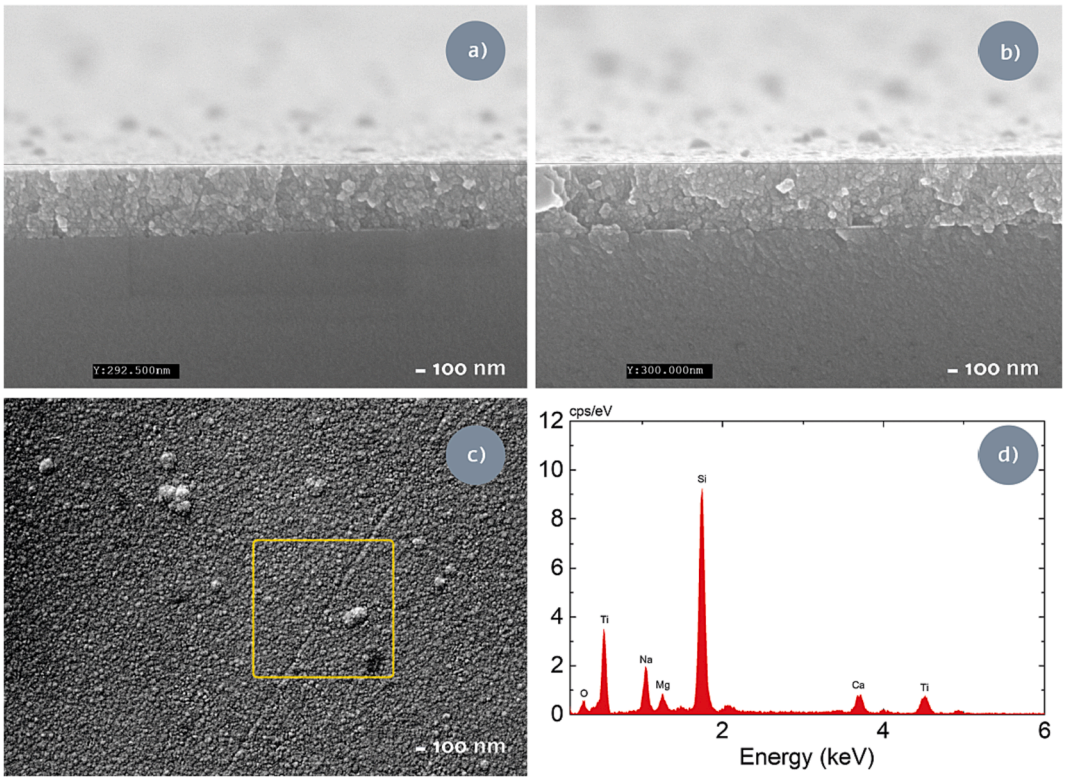

Fig. 3. SEM images for the cross section of(a) TiO_2 transparent thin films, (b) TiO_2-Ag NPs, (c) top surface of TiO_2, and (d) EDS spectra for the surface of TiO_2.

carbon film and left to dry before TEM analysis. Raman studies were conducted using a combined Raman–AFM-SNOM confocal microscope WiTec alpha300 RAS + with an Nd:YAG laser operating at 532 nm (35 mW) and a He:Ne laser operating at 633 nm (25 mW) as excitation sources. Ultraviolet–visible diffuse reflectance spectroscopy (DRS) was measured using a UV–vis spectrophotometer (JASCO U-560 UV–vis spectrophotometer). Fourier transform infrared (FTIR) spectra of the particles were measured in the solid state. The spectra of the materials were collected using a Bruker Optics Tensor 27 spectrometer coupled to a horizontal attenuated total reflectance (ATR) cell using 256 scans at a resolution of 4 cm^{-1}.For the photocatalyst leaching study an ICP-OES Jobin Yvon Activa M was used.

2.3. Synthesis of transparent TiO_2-Ag NPs thin films.

Synthesis of transparent TiO_2 thin films: 2.6 mL of titanium (IV) bis (acetylacetonate) diisopropoxide (75 w.t % in isopropanol) was mixed with 20 mL of EtOH. This mixture of precursors was agited for 1 h to ensure the homogeneity of the solution. The concentration of the final solution was 0.2 M. After mixing for 30 min the solution was applied by hand using a dual action gravity feed airbrush with a flow rate of 5.75 mL/minwas used to apply the solution onto a soda-lime glass substrate (Fig.S1) previously heated to 450 °C. Prior to heating, it was cleaned by introducing the glass into a 30 % (w/w) NH_3 solution and placing them in an ultrasonic bath for 20 min. The thin films thus deposited were then heated to 550 °C under atmospheric pressure on a hot plate to increase their crystallinity and remove any organic residue from the transparent thin film.

Synthesis of Ag NPs: Colloidal NPs were synthesized using the PLAL technique [23,24]. The experimental setup is shown in Fig. S1 and it is based on a home made semi-batch configuration. The main elements are the pulsed laser, the irradiation zone, and the peristaltic pump. The laser irradiation was carried out using the second harmonic of an Nd:YAG pulsed laser (Brilliant, Quantel), with a pulse width of 4 ns full width at half maximum at a fundamental wavelength of 1064 nm and a repetition rate of 10 Hz. A 650 mW mean power laser beam is focused with a 75 mm focal lens (Fig.S2). The irradiation zone is formed by a plastic vessel containing Milli-Q water in which the ultrapure silver foil was immersed. The vessel was attached to a two-dimensional motion-controlled stage moving at a constant speed of 2.5 mm/s in the focus plane perpendicular to the laser beam, where the silver foil was placed, in a raster scanning pattern. To remove nanoparticles and bubbles from the ablation area, and thus enhance productivity, a peristaltic pump (Watson Marlow 323) was used at 60 rpm for the circulation of the 350 mL of water. The irradiation time was of 4 h. This process allowed us to obtain a productivity of 3.1 mg/h. After the fabrication, the concentration of the silver colloid was measured by means of a UV–vis spectroscopy [29] providing a concentration of 11.52 mg/L, which is optimal for use on transparent TiO_2 thin films.

In the fabrication of transparent TiO_2-Ag NPs thin films, a physical assembly was applied to load Ag NPs onto TiO_2 thin films. 2 mL of the water solution of Ag NPs was mixed with 15 mL of EtOH. After mixing the solution for 30 min, it was applied by airbrush. In order to calculate the stabilisation of the Ag NPs, the Zeta Potential technique was used. The Zeta Potential and the stability of Ag NPs vary depending on the pH of the solution where the colloid is prepared. In this case, for a water solution with a pH of 6.9, the ± 30 mV is an important limit for the colloid stability [30]. As can be seen in Fig.S3, the maximum value obtained by this technique was −31.2 mV. This value exceeds the limit established to determine the stability of the NPs. This allows us to ensure that the stability of the Ag NPs colloid is correct. The flow rate was 5.75 mL/min on a soda-lime glass substrate (2.5 × 2.5 cm) previously heated to 250 °C to remove the dispersant and improve the adhesion of NPs on the TiO_2 thin film. The appearance of the transparent TiO_2 and TiO_2-Ag NPs thin films are shown in Fig.S4. The total amount of silver on the surface of the film was 0.0251 mg.

2.4. Photocatalytic screening experiments

The RhB photodegradation experiments were performed under illu-

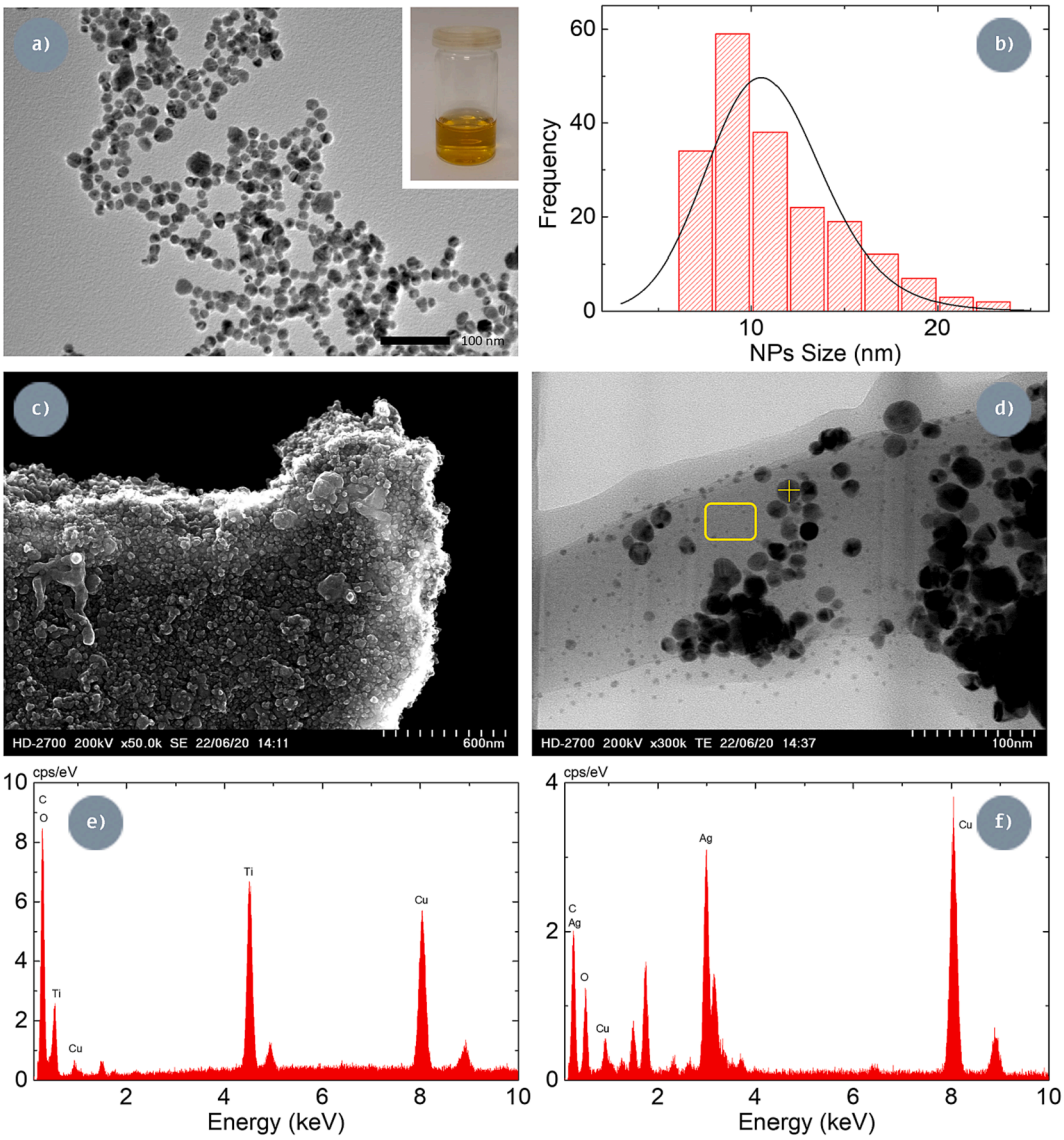

Fig. 4. (a) Conventional TEM image of the Ag NPs before deposition,(b) size distribution of the Ag NPs (c) TEM-SE image of the transparent TiO_2-Ag NPs thin film, (d) Conventional TEM image of the transparent TiO_2-Ag NPs thin film and (e) EDS spectra of the surface of TiO_2 and (f) EDS spectra of the Ag NPs on the surface of TiO_2.

mination using UV light illumination to evaluate the photocatalytic properties of the transparent thin film samples. The prepared thin films (2.5 × 2.5 cm) were immersed in a glass reactor with a 30 mL RhB solution (5 mg/L) and stirred in the dark for 30 min to ensure an dsorption/desorption equilibrium was accomplished. The samples were then placed under UV light lamp (SUPRATECH HTC 150–211 UV, Osram) with a power of 22 W for the UVA wavelength (315–400 nm) and 6 W for the UVB wavelength (280–315 nm). Nominal power was 150 W and light intensity is 0.105 W/cm^2. The experimental set-up of the photocatalysis is shown in Fig.S5. Measurements of the degradation of pollutants exposed to UV light were analyzed every 10 min for the first 30 min and every 30 min afterwards, and the concentration of RhB was monitored by UV–vis spectroscopy at 554 nm, using the following equation (1):

$$\eta(\%) = \left(1 - \frac{C_t}{C_0}\right) \times 100 \quad (1)$$

where C_0 represents the initial RhB concentration and C_t refers to the real time concentrations of RhB, respectively.

The reusability test of the transparent TiO_2 and TiO_2-Ag NPs thin film catalyst was investigated, despite the possibility of the thin film being separated from the glass or leaching of the material into the RhB solution to be photodegraded. For this purpose, the same photodegradation study was carry out with the 5 mg/L solution of RhB using the same catalyst for four and its degradation efficiency (%) was studied.

2.5. *In situ capture experiment*

In situ capture experiments were carried out to investigate the active species generated during the photocatalytic process of TiO_2 and TiO_2-Ag NPs. *tert*-butyl alcohol (*t*-BuOH), formic acid (FA), and 1,4-Benzoquinone (1,4-BQ) were used to capture hydroxyl radicals (OH•), holes (h^+) and superoxide radicals ($O_2^{-\bullet}$), respectively [19,20]. The concentration of the formic acid, 2,4-benzoquinone and *tert*-butyl alcohol were 1 mmol/L in 30 mL reaction solution.

2.6. *Determination of antibacterial activity*

The antibacterial activity of the transparent TiO_2 and TiO_2-Ag NPs thin films was evaluated in accordance with the standard method test

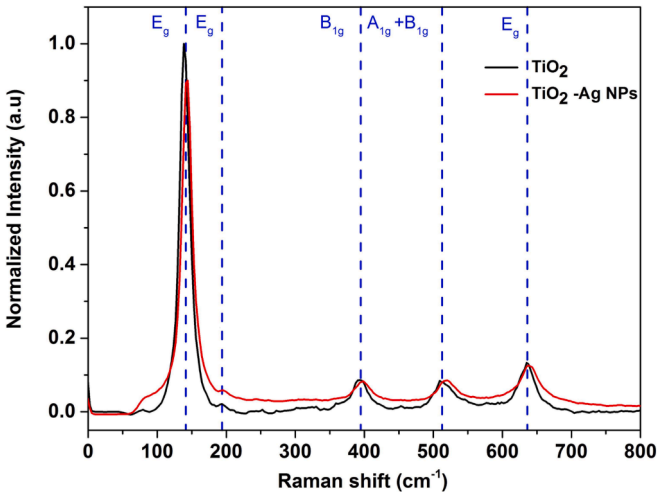

Fig. 5. Raman average spectra of the transparent TiO_2 and TiO_2-Ag NPs thin films.

Table 1
Raman spectra of thin film TiO_2 and TiO_2-Ag NPs normalized to the most intense peak (144 cm^{-1}).

Band Mode	E_g	E_g	B_{1g}	$A_{1g} + B_{1g}$	E_g
Raman shift (cm^{-1})					
TiO_2	138	190	393	509	635
TiO_2-Ag NPs	144	196	398	520	637
TiO_2 (Anatase) [35]	144	197	399	519	639

Jisz 2801_2000, with modifications. *Escherichia coli* ATCC 25922 was used as the reference bacterial strain. Fresh bacterial cells were grown overnight at 37 °C in LB (Luria broth) culture media. A cell suspension (100 μL) of approximately 4 × 10^5 cells/mL was placed over each sample and carefully covered with a film. Reference samples were glass, and TiO_2 treated samples. Samples were then placed under UV light, with an intensity of 0.05 mW/cm^2 for 4 h and viable bacterial cells were quantified by the spread plate method. Two samples of each were tested and three plates were prepared for bacterial counts. Also, as a reference, cell suspension was placed over glass sample, covered with film, and immediately retrieved and plated using the same bacterial cell counts. Plates were incubated for 16 h at 37 °C and colony forming units (CFU) counted.

The antibacterial rate (R) was calculated according to equation (2):

$$(\mathbf{R}) = (N_0 - \mathbf{N})/N_0 \times 100 \quad (2)$$

where N_0 represents the average number of viable bacteria on a reference sample, and N is the average number of bacteria on samples treated with TiO_2-Ag NPs.

3. Results and discussion

3.1. Characterization of transparent TiO_2-Ag NPs thin films

GIXRD analyses of TiO_2 and TiO_2-Ag NPs are shown in Fig. 2. The 2θ values at 25.3, 48.0, 52.8, 55.0, 62.6, and 75.0° are those of the crystalline planes (101), (200), (105), (211), (204) and (215) of the anatase polymorph, based on the file 01–071-1166 of the JCPDS [31,32].Moreover, the peak observed at 44.3° represents to the Ag cubic crystalline phase associated with the crystalline plane (200) based on the file 03–065-2871 of the JCPDS. The peaks corresponding to the silver oxide are also observed at 32.1 and 53.8°, corresponding to the (111) and (220) crystalline planes, based on the file 01–076-1489 of the JCPDS. The partial oxidation of some of the Ag NPs is due to the temperature of the substrate when deposited onto the TiO_2 thin films [33]. The GIXRD results showed that the bulk structure of the anatase was not affected by the Ag NPs, since they were located only on its TiO_2 surface [34].

Fig. 3(a) and Fig. 3(b) show cross-section images of the transparent TiO_2 and TiO_2 Ag NPs thin films. The thickness is the same in both cases, i.e, around 300 nm. The layers formed in them are compact and dense. Fig. 3(c) shows the top surface texture of the TiO_2 films, revealing their continuity. Fig. 3(d) shows EDS spectra for the TiO_2 thin films as well as the composition of the glass on which they are deposited. Elements from the soda-lime glass substrate (Si,Ca,Mg) were also detected.

The TEM images clearly show that the the Ag NPs have been successfully deposited on the transparent TiO_2 thin films. Fig. 4(a) shows conventional TEM images of the NPs obtained by the nanosecond laser before deposition on the TiO_2 thin film. Fig. 4(b) shows the size distribution of the Ag NPs, resulting in a mean size dispersion value of about 10 nm. In Fig. 4(c), we can observe in TEM-SE mode the morphology of the layer once it has been removed from the glass substrate, as well as the great homogeneity and continuity throughout it. Fig. 4(d) shows the deposition of the Ag NPs on the TiO_2 thin film without affecting the macrophology of the NPs, which remain mainly spherical, and the agglomeration can also be observed once they adhere to the TiO_2 surface. Fig. 4(e) and Fig. 4(f) show the corresponding EDS spectra for the areas where only Ag NPs are present and the area where only the TiO_2 layer is present. The Cu and C that appear in the spectrum come from the grids where the material to be analyzed has been deposited.

Raman spectroscopy was utilized to further study the structure of the transparent thin films. The Raman spectra of the samples confirmed anatase as the only TiO_2 phase present in the surfaces of the thin films'. The normalized (over the most intense band at approx. 138 cm^{-1}) average spectra of the particular clusters are presented in Fig. 5, while detailed assignments of the bands are shown in Table 1. The minimal differences in the values of the Raman shift between the TiO_2 and TiO_2-Ag NPs layers are related to the compression of the layers and are not due to the interaction of the Ag NPs with the TiO_2 [35].

3.2. Optical spectral properties of TiO_2 and TiO_2- Ag NPs transparent thin films

The results of the optical properties of the transparent thin films were characterized using UV–vis absorption spectroscopy. As shown in Fig. 6 (a), the thin films have a high transmittance of up to 85 % in the case of TiO_2 and 80 % when loaded with Ag NPs.The oscillations observed in the transmittance spectrum are due to interferences between the interface of the glass with the thin film and the thin film with the air [36]. Fig. 6(b) shows the absorption spectra for the transparent TiO_2 and TiO_2-Ag thin films with the maximum absorption occurring in the UV. Bandgap values for each film were also obtained,from the transmittance results (see Fig. 5(c)). To do so, first, the absorption coefficient (α) values were calculated using Lambert's Law as the following equation (3) [37]:

$$A = \frac{1}{t}\ln\left(\frac{1}{T}\right) \quad (3)$$

where T is the transmittance, and t is the film thickness. An optical bandgap of thin films was estimated using equation (4) by the extrapolation of $(\alpha h\nu)^2$ vs $h\nu$.

$$\alpha h\upsilon = A\left(h\upsilon - E_g\right)^{\frac{1}{2}} \quad (4)$$

where A is a constant, hv is the photon energy, and Eg is the optical bandgap. The optical bandgap of transparent TiO_2 and TiO_2-Ag NPs thin films was determined by extrapolating the region of the plot to the energy axis where $\alpha^2 = 0$, and was found to have a value of 2. The band gap

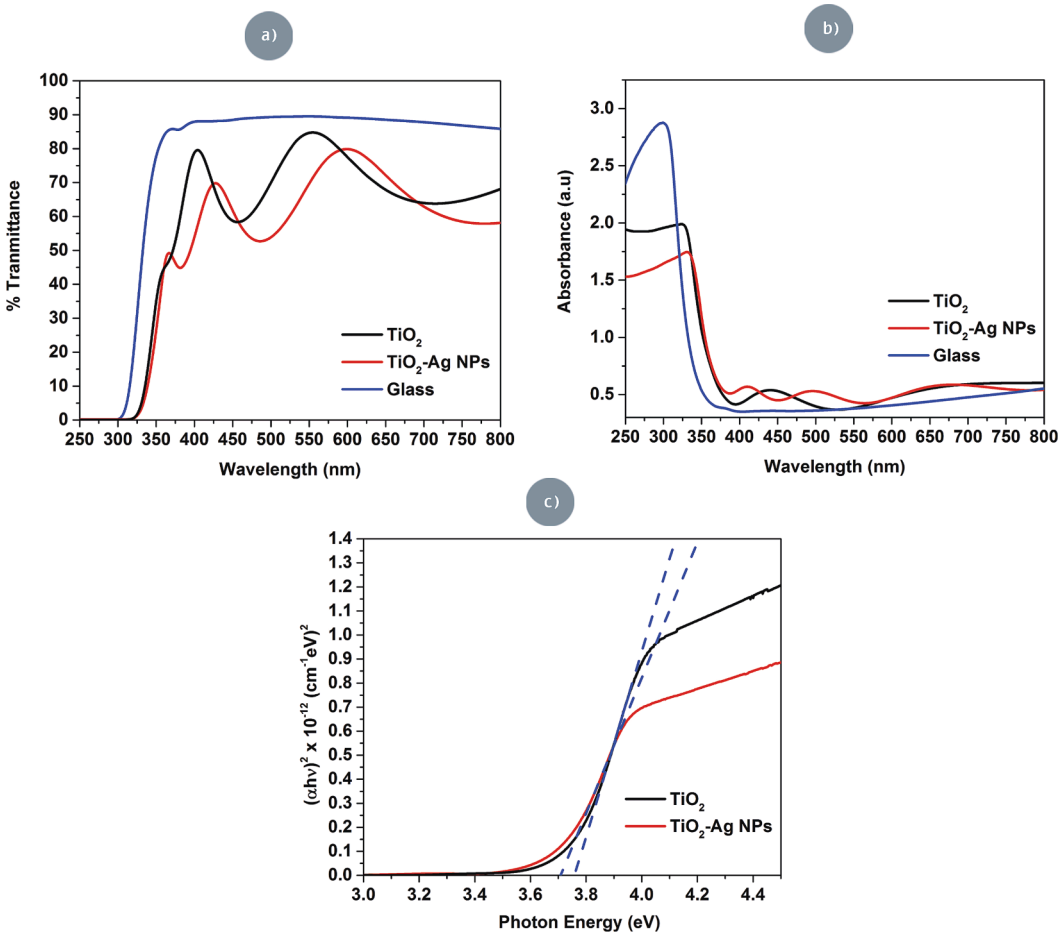

Fig. 6. (a) The transmittance, (b) the absorbance and (c) the optical band gap of transparent TiO_2 and TiO_2-Ag NPs thin films.

value for the TiO_2 thin films was 3.758 eV, whereas for the TiO_2-Ag NPs it showed a small decrease with a band gap value of 3.708 eV. This small variation was due to the fact that the NPs were on the surface of the TiO_2 thin film and not inserted/doped into the TiO_2 structure, where considerable changes in the band gap value should be expected [38]. Moreover, this variation may also be due to changes in grain size, a specific surface area or the microstructure of the thin films [36]. Thickness is also a variable but in this case both TiO_2 and TiO_2-Ag thin films had very similar thicknesses.

3.3. Applications of transparent TiO_2 and TiO_2- Ag NPs thin films

Compared to other transparent thin films, TiO_2-Ag NPs show very high optical properties. By taking advantage of other thin film layers, several applications including photocatalysis and antimicrobial surfaces were performed with TiO_2-Ag NPs.

3.3.1. Photocatalytic degradation of RhB

The photocatalytic activity of the thin films was assessed initially by monitoring the degradation of RhB solutions irradiated with UV light. A series of experiments were then conduced to evaluate the photocatalytic degradation of transparent TiO_2 and TiO_2-Ag NPs thin films. First, the photodegradation of RhB in the absence of the thin films was evaluated in two control assays: (i) under UV-light radiation, and (ii) under UV-light irradiation and the presence of a glass substrate. The results showed that 16 % and 15.6 % of RhB were degraded after 330 min in the blank experiments (i) and (ii), respectively (Fig.S7). Moreover, the capacity of thin films to adsorb RhB molecules was also evaluated, using TiO_2 and TiO_2-Ag NPs thin films under dark conditions. It was found that a very low amount of RhB was adsorbed on the surface of the thin films (about 14 %) (Fig.S6), reaching the maximum plateau at 30 min.

The total weight was 0.9 mg for both TiO_2 and TiO_2-Ag NPs thin films. In addition, the amount of catalyst was much smaller than similar work published in the literature [39,40]. UV–vis absorption spectra of RhB dye degradation using TiO_2 are shown in Fig.S8. The thin films of TiO_2 degraded 85.3 % in 210 min whereas TiO_2-Ag NPs thin films were able to degrade 99.4 % in the same time as shown in Fig. 7(a). Fig. 7(b) also clearly shows the difference in photodegradation efficiency by representing the C/C_0 for the transparent of TiO_2 and TiO_2-Ag NPs thin films, together the experimental points obtained and the mathematical fit to an exponential. The calibration line used to obtain the concentration values is shown in Fig.S9. This difference in the photodegradation between TiO_2 thin films and TiO_2-Ag NPs is due to the fact that Ag NPs on the TiO_2 surface cause an equilibrium of the Fermi energy level that leads to the bending of the semiconductor's CB, thereby generating a Schottky junction. This in turn promotes the transfer of photo-excited electrons from the CB of TiO_2 to Ag, thus preventing the recombination of electron-hole pairs (e^-/h^+) in the TiO_2 matrix. These electrons can be combined with oxygen to generate the superoxide radicals, which can further combine with holes to yield higher hydroxyl radicals (than when it occurs only on the TiO_2 surface) [41,42].

TheThe kinetics of RhB decontamination was performed using the expression presented in equation (5):

$$k_{app} = \frac{-\ln\left(\frac{C}{C_0}\right)}{t} \quad (5)$$

where k_{app} (min^{-1}) represents the reaction rate constant in min^{-1} at time t (min). As can be seen in Fig. 7(c), when TiO_2 thin film is in contact

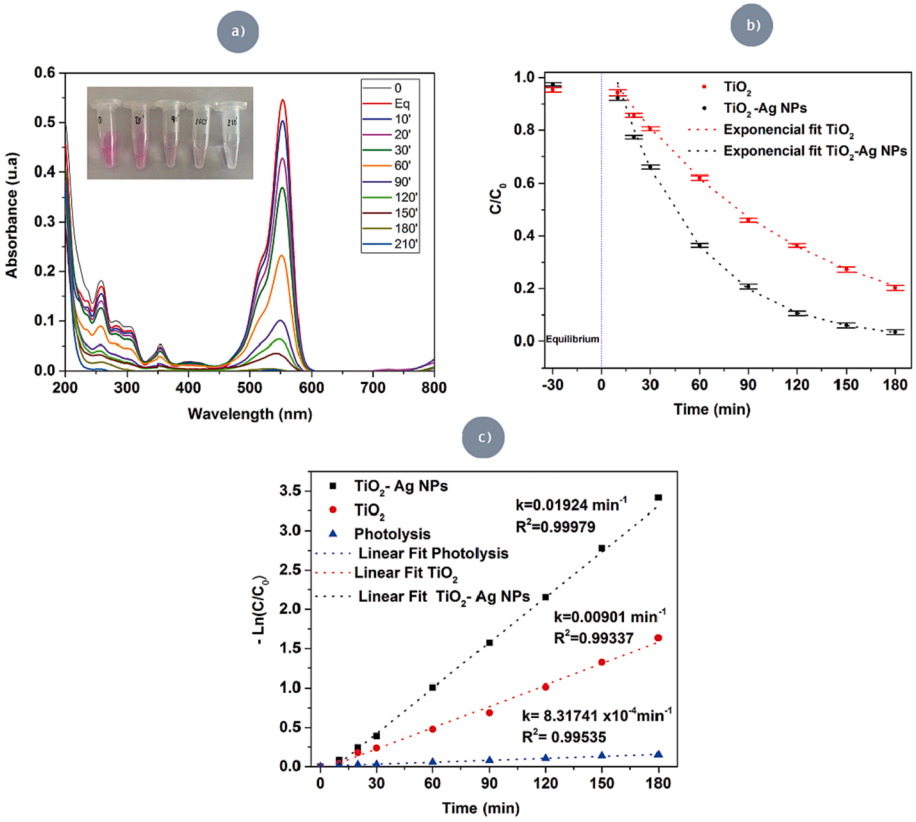

Fig. 7. (a) UV–vis absorption spectra of aqueous solutions of RhB (C_0 = 5 mg/L) under UV-light irradiation in the presence of TiO_2-Ag NPs thin films; (b) Photodegradation performance and (c) respective Curve of pseudo-first-order decay fitted linear regression, for RhB photodegradation in the presence of TiO_2-Ag NPs and TiO_2 thin films.

Table 2
Comparison of the transparent TiO_2-Ag NPs thin films with other recent similar photocatalytic thin films under UV light.

Samples	Dye concentration (mg/L)	Removal	Kapp (10^{-3} min^{-1})
This work	5.0 RhB	99.7 % after 3.5 h	19.1
Cu doped-ZnO [43]	3.2 Metylene Blue (MB)	74.0 % after 2 h	5.6
TiO_2 [44]	10.0 MB	53.06 % after 2 h	4.1
0.05Fe_2O_3/TiO_2 [45]	4.79 RhB	60 % afte 5 h	–
Ag loaded TiO_2-ZnO [46]	10.0 MB	70 % after 2 h	9.92

with Ag NPs the kinetic costant is twice as high as when the reaction takes place with TiO_2 alone. The value of the constant for the TiO_2 is 9.01×10^{-3} while the value for the TiO_2-Ag NPs thin films is 19.14×10^{-3} min^{-1}.This kinetic constant value is much higher than the costant values obtained for the degradation of differents dye concentrations by different compounds also in thin films as shown in Table 2 [33–36].

As shown in Fig. 8(a), after adding *tert*-butyl alcohol to the reaction solution, the photocatalytic degradation rate of the RhB solution decreased from 99.70 % to 55.8 %.,while adding FA or 1,4-BQ only decreased the degradation rate to 82.45 % and 71.77 % respectively. Fig. 8(b) shows a bar graph representing the photocatalytic degradation using each of the radical scavengers. Fig. 8(a) and 8(b) indicate that the holes (h^+) make a limited contribution to RhB removal and also reveal that $O_2^{\bullet-}$ played an insignificant role through the degradation process, thus confirming that OH• played a crucial role in the process. The schematic representation of the photo-generated charge transfer process in transparent TiO_2-Ag NPs thin films under UV is illustrated in Fig. 8(c) and Eqs. (6)–(14) [47–49].

$$TiO_2 + hv_{UV} \rightarrow TiO_2 + (e^- + h^+) \quad (6)$$

$$h_{UV} + H_2O \rightarrow H^+ + OH^- \quad (7)$$

$$e^-_{CB} + O_2 \rightarrow O_2^- \quad (8)$$

$$O_2^- + H^+ \rightarrow HO_2 \quad (9)$$

$$HO_2 + e^-_{CB} \rightarrow H_2O_2 \quad (10)$$

$$H_2O_2 + e^-_{CB} \rightarrow OH^- + OH\cdot \quad (11)$$

$$OH^- + hv_{UV} \rightarrow OH\cdot \quad (12)$$

$$Ag + e^-_{CB-TiO_2} \rightarrow Ag + e^-_{CB} \quad (13)$$

$$O_2 + > H_2O + e^-_{CB} \rightarrow OH\cdot \quad (14)$$

This mechanism explains how, under UV irradiation, hole-electron pairs are photogenerated in TiO_2 thin film. The CB level of TiO_2 is higher than the Fermi energy level of Ag NPs, so the photoexcited electrons from TiO_2 are transferred to the Ag NPs, acting as electron scavengers for TiO_2 [47]. In this way, the recombination of electrons and photoinduced holes is reduced and the lifetime is prolonged. This explains the results obtained, the photodegradation of RhB is much faster as the hydroxyl radical species have a longer lifetime due to the Ag NPs, thus achieving a faster photodegradation of the dye.

In order to study the durability and reusability of these thin films as photocatalysts, they were subjected to cyclic tests, that were run four times. Fig. 9(a) shows the photocatalytic degeneration of RhB on these

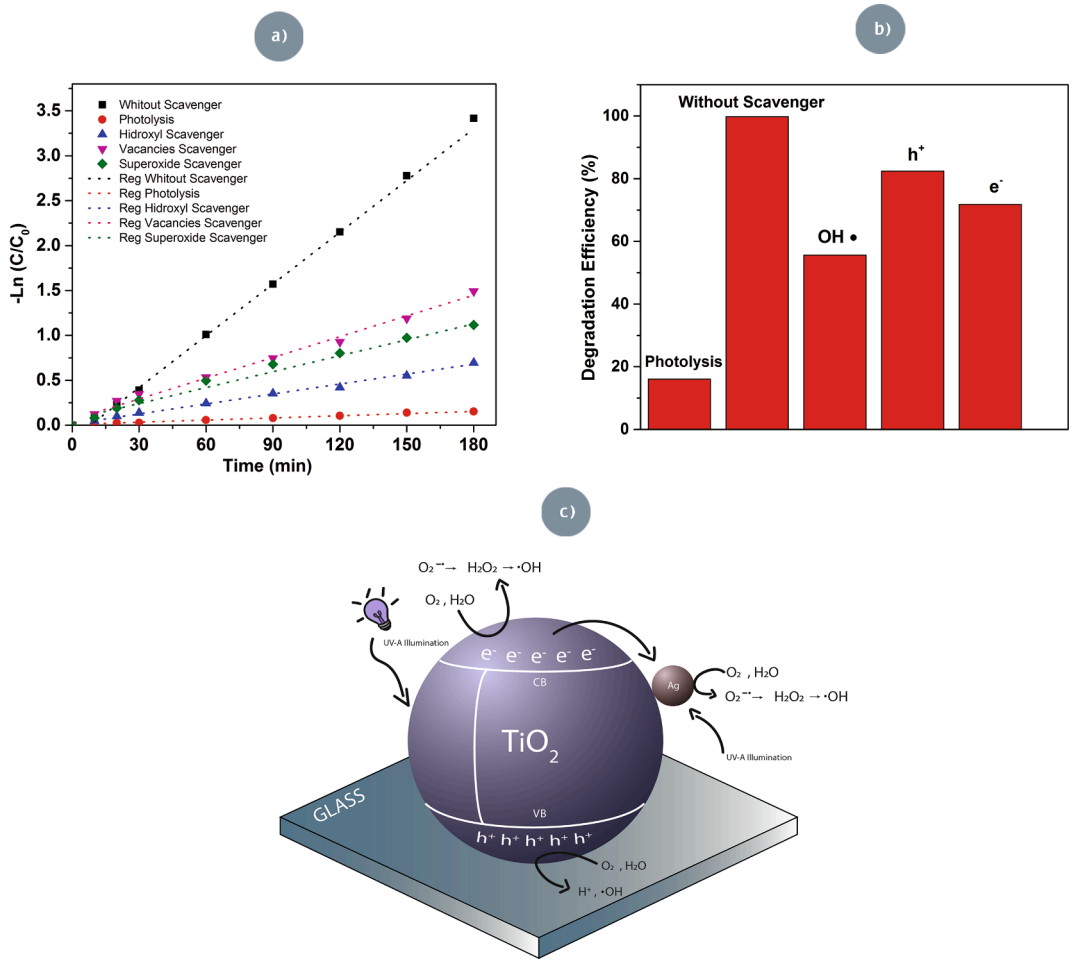

Fig. 8. (a) Reaction kinetics of the photoreaction with various scavengers on TiO_2-Ag NPs; (b) Degradation Efficiency (%) with various scavengers on TiO_2-Ag NPs; (c) The degradation mechanism of transparent TiO_2-Ag NPs thin films.

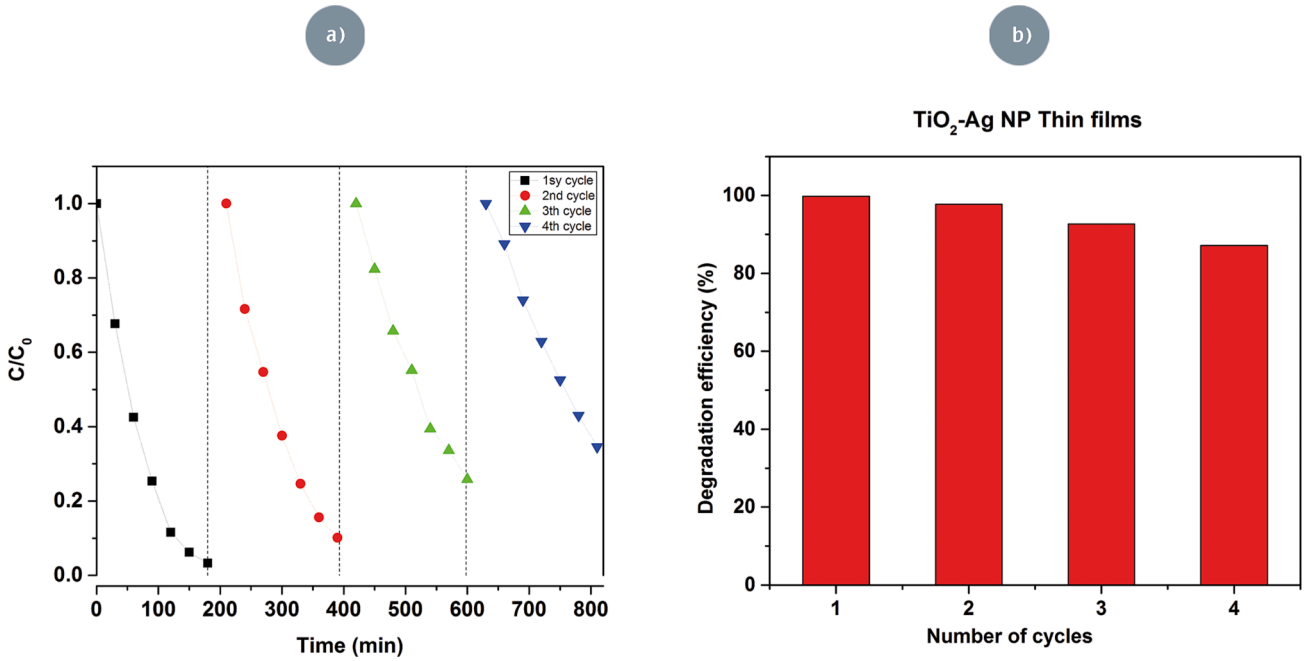

Fig. 9. (a) Reusability of the transparent TiO_2-Ag NPs thin films in the photocatalytic degradation of RhB under UV light irradiation after four cycles, and (b) bar graph of the percentage of degradation efficiency over four cycles.

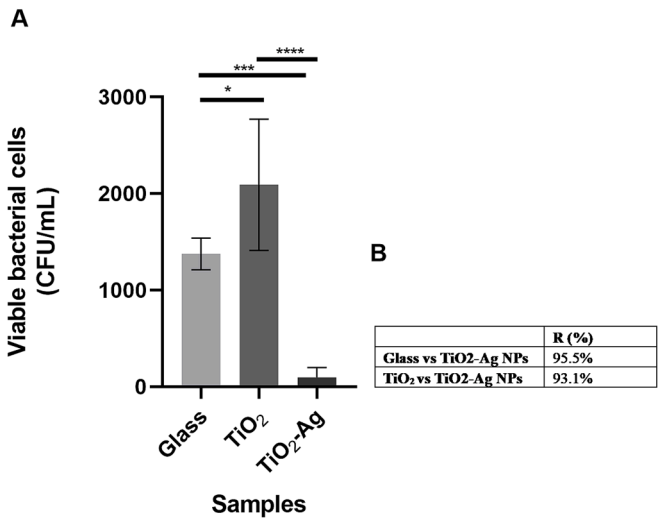

Fig. 10. Antibacterial assay of transparent TiO_2-Ag NPs thin films (a) Results of colony forming units/mL (CFU/mL) in each sample tested. Significance (*) of the results was verified using one-way ANOVA **then** Sidak's multiple comparisons test was used to determine statistical significance. (b) Antibacterial rates (%) obtained for TiO_2-Ag NPs compared with glass and with TiO_2 samples.

thin films after four cycles. After four cycles the TiO_2-Ag NPs photocatalyst had only lost an efficiency from 99.77 % to 87.16 % as can be seen in the bar chart in Fig. 9(b). This decrease in efficiency is due to the fact that RhB is adsorbed after cycling on the active centers of the photocatalyst causing a slight decrease in degradation efficiency as can be seen in the FTIR spectra (Fig. S10) where after four cycles we can see the characteristic bands of RhB (3385 cm^{-1}, 2922 cm^{-1}, 2850 cm^{-1} and 1635 cm^{-1}) on the photocatalyst. For the stability study of the photocatalyst, the possible presence of Ag and Ti was also measured during the photocatalysis tests in the RhB solution using an internal method based on ISO 11885. The results obtained for 0, 210 and 300 min show that the amount of Ag and Ti was always below the detection limit of the technique (Table S.1), thus confirming that there was no leaching of metals into the RhB solution.

3.3.2. Antibacterial activity of transparent TiO_2-Ag NPs thin films.

The antibacterial activity of transparent TiO_2-Ag NPs thin films was determined in accordance with standard tests JISZ 2801_2000 after exposure to UV light for 4 h. Glass, TiO_2 and TiO_2-Ag NPs samples were used as a reference and suspended Gram-negative E. coli ATCC 25922 cells were placed on each sample. After counting viable cells recovered from the surface of the materials, antibacterial rates were calculated. Results are presented in Fig. 10 and clearly show a strong antibacterial action of TiO_2-Ag NPs, when compared with glass and with TiO_2 samples,with values of 95.5 % and 93.1 %, respectively. Results are significantly different are marked with (*) in Fig. 10. The differences observed for both controls, glass and TiO_2 samples, are probably due to slightly different material performances in the complete recovery of treated bacterial cells form the surface of materials. These differences do not preclude the strong antibacterial action observed.

4. Conclusion

Pure and TiO_2-Ag NPs transparent thin films with Ag NPs synthesized by nanosecond laser, with excellent photocatalytic activities being obtained for the degradation of RhB using UV light for a very small amount of catalyst, maintaining a very high degree of glass transparency of more than 80 %. Thanks to the Ag NPs, it was observed that the production of radicals (OH•) increased,as did the lifetime, which made the degradation of the dye much faster and up to 99.7 % of the dye could be degraded in 210 min. The removal efficiency for RhB reached 99.7 %, which was twice than that of pure TiO_2. Furthermore, the reuse of the catalyst for four cycles was also studied, observing that the degradation efficiency decreased by 10 %.These results are very interesting due to the fact that the catalyst is synthesized on glass by using methodologies, that are widely applicable in industry the result being a catalyst with a high degradation efficiency for pollutants and dyes such as RhB. Also, the films that were developed, after addition of Ag NPs to the surface, showed strong antibacterial activities, as measured using a gram-negative bacterium as reference strain. The reduction in the number of bacteria reached 93 % after irradiation under UV-light for 4 h. Further research could measure the antimicrobial power of these transparent thin films by the addition of Ag NPs to the surface as well as the photocatalytic action of the films using different types of light (visible light or sunlight). Additionally, the combination of these two techniques would allow an the easy synthesis of a multitude of compounds that can be functionalized with metal NPs.

CRediT authorship contribution statement

J.G. Cuadra: Investigation, Writing – original draft, Writing – review & editing. **S. Molina-Prados:** Investigation, Writing – original draft, Writing – review & editing. **Gladys Mínguez-Vega:** Investigation, Writing – original draft, Writing – review & editing. **Ana.C. Estrada:** Investigation, Writing – original draft, Writing – review & editing. **T. Trindade:** Methodology, Resources, Writing – review & editing. **C. Oliveira:** Investigation, Writing – original draft, Writing – review & editing. **M.P. Seabra:** Validation, Supervision. **J. Labrincha:** Methodology, Resources, Writing – review & editing. **S. Porcar:** Investigation, Writing – original draft, Writing – review & editing. **R. Cadena:** Writing – original draft, Writing – review & editing. **D. Fraga:** Methodology, Resources, Writing – review & editing. **J.B. Carda:** Validation, Supervision.

Declaration of Competing Interest

The authors declare that they have no known competing financial interests or personal relationships that could have appeared to influence the work reported in this paper.

Data availability

No data was used for the research described in the article.

Acknowledgements

The authors would like to acknowledge the financial support of the Spanish Ministry of Economy and Competitiveness under the Ministry of Science and Innovation "R& D& I Projects" of the State Programs for the Generation of Knowledge and Scientific and Technological Strengthening of the R& D& I System and R& D& I Oriented towards the Challenges of Society, within the framework of the Spanish National Plan for Scientific and Technical Research and Innovation (2019-2020) project PID2020-116719RB-C43 financed by MCIN/ EAI/ 10.13039/501100011033.

This work also has also been funded by project PID2019-110927RB-I00 financed by MCIN/AEI/10.13039/501100011033. Funding from the Generalitat Valenciana (PROMETEO/2020/029) and the Universitat Jaume I (UJI-B2019-37) is also acknowledged. The authors are very grateful to the "Serveis Centrals d'Instrumentación Científica" (SCIC) of the Universitat Jaume I for the use of lasers and for the assistance in the characterization of the materials. This work was also developed within the scope of the project CICECO-Aveiro Institute of Materials, UIDB/50011/2020, UIDP/50011/2020 & LA/P/0006/2020, financed by national funds through the FCT/MCTES (PIDDAC). Ana C. Estrada also acknowledges the costs of her research contract resulting from the FCT hiring funded by National funds (OE), through FCT, I.P., in the scope of

the framework contract foreseen in points 4, 5, and 6 of Article 23 of the Decree-Law 57/2016, of 29 August, amended by Law 57/2017, of 19 July.

Appendix A. Supplementary data

Supplementary data to this article can be found online at https://doi.org/10.1016/j.apsusc.2023.156519.

References

[1] C. Doroody, K.S. Rahman, T.S. Kiong, N. Amin, Optoelectrical impact of alternative window layer composition in CdTe thin film solar cells performance, Sol. Energy. 233 (2022) 523–530, https://doi.org/10.1016/j.solener.2022.01.049.

[2] S. Tyagi, A. Kumar, A. Kumar, Y.K. Gautam, V. Kumar, Y. Kumar, B.P. Singh, Enhancement in the sensitivity and selectivity of Cu functionalized MoS2 nanoworm thin films for nitrogen dioxide gas sensor, Mater. Res. Bull. 150 (2022), 111784, https://doi.org/10.1016/j.materresbull.2022.111784.

[3] P. Ni, B. Chen, X. Wei, Effects of annealing temperatures on energy storage performance of sol-gel derived (Ba0.95, Sr0.05) (Zr0.2, Ti0.8) O3 thin films, Ceram. Int. (2022), https://doi.org/10.1016/j.ceramint.2022.03.167.

[4] S.A. Khalate, S.A. Kadam, Y.R. Ma, S.B. Kulkarni, V.G. Parale, U.M. Patil, Binder free cobalt iron phosphate thin films as efficient electrocatalysts for overall water splitting, J. Colloid Interface Sci. 613 (2022) 720–732, https://doi.org/10.1016/j.jcis.2022.01.015.

[5] N. Kalangadan, A.S. Mary, R.H. Jyothi, S. Punniyakoti, S. Sundaresan, R. K. Alagarsamy, K. Rajaram, Characterization and antimicrobial evaluation of green synthesized silver nanoparticle thin films with reusable applications, Mater. Lett. 314 (2022), 131923, https://doi.org/10.1016/j.matlet.2022.131923.

[6] S. Chen, T. Liang, N. Wen, F.H. Liu, C.C. Tsao, C.Y. Hsu, Electro-less plating nickel-phosphorus of low carbon steel using various pretreatments and an external magnetic field, J. Saudi Chem. Soc. 24 (2020) 704–714, https://doi.org/10.1016/j.jscs.2020.07.008.

[7] A.C. Alves, F. Wenger, P. Ponthiaux, J.P. Celis, A.M. Pinto, L.A. Rocha, J.C. S. Fernandes, Corrosion mechanisms in titanium oxide-based films produced by anodic treatment, Electrochim. Acta. 234 (2017) 16–27, https://doi.org/10.1016/j.electacta.2017.03.011.

[8] S.I. Dorovskikh, D.D. Klyamer, A.M. Makarenko, K.V. Zherikova, A. E. Turgambaeva, Y.V. Shevtsov, D.B. Kal'nyi, I.K. Igumenov, N.B. Morozova,, The comprehensive study of thermal properties of tris(2,2,6,6-tetramethyl-3,5-heptanedionato)cobalt(III) related to the chemical vapor deposition of Co-oxide based thin film materials, Vacuum. 199 (2022), 110969, https://doi.org/10.1016/j.vacuum.2022.110969.

[9] N.R. Aswathy, J.J. Varghese, S.R. Nair, R.V. Kumar, Structural, optical, and magnetic properties of Mn-doped NiO thin films prepared by sol-gel spin coating, Mater. Chem. Phys. 282 (2022), 125916, https://doi.org/10.1016/j.matchemphys.2022.125916.

[10] K. Vijayan, S.P. Vijayachamundeeswari, K. Sivaperuman, N. Ahsan, T. Logu, Y. Okada, A review on advancements, challenges, and prospective of copper and non-copper based thin-film solar cells using facile spray pyrolysis technique, Sol. Energy. 234 (2022) 81–102, https://doi.org/10.1016/j.solener.2022.01.070.

[11] S.A. Tepe, M. Danışman, N. Cansever, Crystallization of TiO2 on sputter deposited amorphous titanium thin films, Mater. Chem. Phys. 282 (2022), https://doi.org/10.1016/j.matchemphys.2022.125965.

[12] C. Zhang, T. Uchikoshi, T. Ishigaki, Effect of crystalline orientation on photocatalytic performance for Nb-doped TiO2 nanoparticles, Adv. Powder Technol. 32 (2021) 4149–4154, https://doi.org/10.1016/j.apt.2021.09.019.

[13] R.S. Santiago, L.C.D. Silva, F.D. Origo, C. Stegemann, I.L. Graff, R.G. Delatorre, D. A. Duarte, Target power influence on optical and electrical properties of amorphous titanium oxide deposited by reactive grid-assisted magnetron sputtering, Thin Solid Films. 700 (2020), https://doi.org/10.1016/j.tsf.2020.137917.

[14] S. Na-Phattalung, D.J. Harding, P. Pattanasattayavong, H. Kim, J. Lee, D. W. Hwang, T.D. Chung, J. Yu, Band gap narrowing of TiO2 nanoparticles: A passivated Co-doping approach for enhanced photocatalytic activity, J. Phys. Chem. Solids. 162 (2022), 110503, https://doi.org/10.1016/j.jpcs.2021.110503.

[15] M. Balamurugan, M. Silambarasan, S. Saravanan, T. Soga, Synthesis of anatase and rutile mixed phase titanium dioxide nanoparticles using simple solution combustion method, Phys. B Condens. Matter. 638 (2022), 413843, https://doi.org/10.1016/j.physb.2022.413843.

[16] A.H. Shah, M.A. Rather, Effect of calcination temperature on the crystallite size, particle size and zeta potential of TiO2nanoparticles synthesized via polyol-mediated method, Mater. Today Proc. 44 (2021) 482–488, https://doi.org/10.1016/j.matpr.2020.10.199.

[17] H. Peng, S. Xie, P. Niu, Z. Zhang, T. Yuan, Z. Ren, X. Wang, Y. Zhao, R. Li, Jo rn a l P ro of, J. Alloys Compd. (2020), 158286, https://doi.org/10.1016/j.ijleo.2022.169231.

[18] C. Pragathiswaran, C. Smitha, B.M. Abbubakkar, P. Govindhan, N.A. Krishnan, Synthesis and characterization of TiO2/ZnO-Ag nanocomposite for photocatalytic degradation of dyes and anti-microbial activity, Mater. Today Proc. 45 (2021) 3357–3364, https://doi.org/10.1016/j.matpr.2020.12.664.

[19] T. Liu, L. Wang, X. Lu, J. Fan, X. Cai, B. Gao, R. Miao, J. Wang, Y. Lv, Comparative study of the photocatalytic performance for the degradation of different dyes by ZnIn2S4: adsorption, active species, and pathways, RSC Adv 7 (2017) 12292–12300. https://doi.org/10.1039/c7ra00199a.

[20] J.T. Schneider, D.S. Firak, R.R. Ribeiro, P. Peralta-Zamora, Use of scavenger agents in heterogeneous photocatalysis: truths, half-truths, and misinterpretations, Phys. Chem. Chem. Phys. 22 (2020) 15723–15733. https://doi.org/10.1039/d0cp02411b.

[21] Y. Hou, A. Mushtaq, Z. Tang, E. Dempsey, Y. Wu, Y. Lu, C. Tian, J. Farheen, X. Kong, M.Z. Iqbal, ROS-responsive Ag-TiO2 hybrid nanorods for enhanced photodynamic therapy of breast cancer and antimicrobial applications, J. Sci. Adv. Mater. Devices. 7 (2022), 100417, https://doi.org/10.1016/j.jsamd.2022.100417.

[22] S. Barcikowski, V. Amendola, G. Marzun, C. Rehbock, S. Reichenberger, D. Zhang, B. Gökce, Handbook of Laser Synthesis of Colloids (2016). https://doi.org/10.17185/duepublico/41087.

[23] R.C. Forsythe, C.P. Cox, M.K. Wilsey, A.M. Müller, Pulsed Laser in Liquids Made Nanomaterials for Catalysis, Chem. Rev. 121 (2021) 7568–7637, https://doi.org/10.1021/acs.chemrev.0c01069.

[24] D. Zhang, B. Gökce, S. Barcikowski, Laser Synthesis and Processing of Colloids: Fundamentals and Applications, Chem. Rev. 117 (2017) 3990–4103, https://doi.org/10.1021/acs.chemrev.6b00468.

[25] V. Amendola, D. Amans, Y. Ishikawa, N. Koshizaki, G. Compagnini, S. Reichenberger, S. Barcikowski, Room-Temperature Laser Synthesis in Liquid of Oxide , Metal-Oxide Core-Shells , and Doped Oxide Nanoparticles, (n.d.). https://doi.org/10.1002/chem.202000686.

[26] R. Streubel, S. Barcikowski, B. Gökce, Continuous multigram nanoparticle synthesis by high-power, high-repetition-rate ultrafast laser ablation in liquids, Opt. Lett. 41 (2016) 1486, https://doi.org/10.1364/ol.41.001486.

[27] C. Don, R. Torres-mendieta, A. Pyatenko, E. Falomir, M. Ferna, M. Gladys, Fabrication by Laser Irradiation in a Continuous Flow Jet of Carbon Quantum Dots for Fluorescence, Imaging (2018), https://doi.org/10.1021/acsomega.7b02082.

[28] C. Doñate-buendía, M. Fernández-alonso, J. Lancis, G. Mínguez-vega, Overcoming the barrier of nanoparticle production by femtosecond laser ablation in liquids using simultaneous spatial and temporal focusing, Photonics Res. 7 (2019) 1249, https://doi.org/10.1364/PRJ.7.001249.

[29] M. Sikder, J.R. Lead, G.T. Chandler, M. Baalousha, Science of the Total Environment A rapid approach for measuring silver nanoparticle concentration and dissolution in seawater by UV – Vis, Sci. Total Environ. 618 (2018) 597–607, https://doi.org/10.1016/j.scitotenv.2017.04.055.

[30] C.V. Restrepo, C.C. Villa, Synthesis of silver nanoparticles, influence of capping agents, and dependence on size and shape: A review, Environ. Nanotechnology, Monit. Manag. 15 (2021), https://doi.org/10.1016/j.enmm.2021.100428.

[31] A.S. AlShammari, M.M. Halim, F.K. Yam, N.H.M. Kaus, Synthesis of Titanium Dioxide (TiO2)/Reduced Graphene Oxide (rGO) thin film composite by spray pyrolysis technique and its physical properties, Mater. Sci. Semicond. Process. 116 (2020), 105140, https://doi.org/10.1016/j.mssp.2020.105140.

[32] X. Zhang, M. Kamali, T. Ueleners, J. Aymus, Z. Liu, M.E.V. Costa, L. Appels, D. Cabooter, UV/TiO2/Periodate System for the Degradation of Organic Pollutants – Kinetics, Mechanisms and Toxicity Study, Chem. Eng. J. (2022), 137680, https://doi.org/10.1016/j.cej.2022.137680.

[33] N. Fleitas-Salazar, E. Silva-Campa, S. Pedroso-Santana, J. Tanori, M.R. Pedroza-Montero, R. Riera, Effect of temperature on the synthesis of silver nanoparticles with polyethylene glycol: new insights into the reduction mechanism, J. Nanoparticle Res. 19 (2017), https://doi.org/10.1007/s11051-017-3780-3.

[34] R. Lu, J. Sha, W. Xia, Y. Fang, L. Gu, Y. Wang, A 3D-SERS substrate with high stability: Silicon nanowire arrays decorated by silver nanoparticles, CrystEngComm. 15 (2013) 6207, https://doi.org/10.1039/c3ce40788h.

[35] M. Lubas, J.J. Jasinski, M. Sitarz, L. Kurpaska, P. Podsiad, J. Jasinski, Raman spectroscopy of TiO2 thin films formed by hybrid treatment for biomedical applications, Spectrochim. Acta - Part A Mol. Biomol. Spectrosc. 133 (2014) 867–871. https://doi.org/10.1016/j.saa.2014.05.045.

[36] D. Komaraiah, E. Radha, J. Sivakumar, M.V. Ramana Reddy, R. Sayanna, Structural, optical properties and photocatalytic activity of Fe3+ doped TiO2 thin films deposited by sol-gel spin coating, Surfaces and Interfaces. 17 (2019), 100368, https://doi.org/10.1016/j.surfin.2019.100368.

[37] T. Ratana, P. Amornpitoksuk, T. Ratana, S. Suwanboon, The wide band gap of highly oriented nanocrystalline Al doped ZnO thin films from sol-gel dip coating, J. Alloys Compd. 470 (2009) 408–412, https://doi.org/10.1016/j.jallcom.2008.02.081.

[38] D. Komaraiah, E. Radha, J. Sivakumar, M.V. Ramana Reddy, R. Sayanna, Photoluminescence and photocatalytic activity of spin coated Ag+ doped anatase TiO2 thin films, Opt. Mater. (Amst). 108 (2020), 110401, https://doi.org/10.1016/j.optmat.2020.110401.

[39] B. Xing, C. Shi, C. Zhang, G. Yi, L. Chen, H. Guo, G. Huang, J. Cao, Preparation of TiO2/Activated Carbon Composites for Photocatalytic Degradation of RhB under UV Light Irradiation, J. Nanomater. 2016 (2016), https://doi.org/10.1155/2016/8393648.

[40] T. Wang, T. Tang, Y. Gao, Q. Chen, Z. Zhang, H. Bian, Hydrothermal preparation of Ag-TiO2-reduced graphene oxide ternary microspheres structure composite for enhancing photocatalytic activity, Phys. E Low-Dimensional Syst. Nanostructures. 112 (2019) 128–136, https://doi.org/10.1016/j.physe.2018.10.033.

[41] D.S. Liu, J. Wu, Y. Wang, H. Ji, L. Gao, X. Tong, M. Usman, P. Yu, Z. Wang, Tailored performance of layered transition metal dichalcogenides via integration with low dimensional nanostructures, RSC Adv. 7 (2017) 11987–11997, https://doi.org/10.1039/c7ra01363a.

[42] F. Mo, Q. Zhou, Y. He, Nano–Ag: Environmental applications and perspectives, Sci. Total Environ. 829 (2022), 154644, https://doi.org/10.1016/j.scitotenv.2022.154644.

[43] F.Z. Nouasria, D. Selloum, A. Henni, S. Tingry, J. Hrbac, Improvement of the photocatalytic performance of ZnO thin films in the UV and sunlight range by Cu doping and additional coupling with Cu2O, Ceram. Int. 48 (2022) 13283–13294, https://doi.org/10.1016/j.ceramint.2022.01.207.
[44] A. Kumar, V.K. Saxena, R. Thangavel, B. Kumar, A dual effect of surface roughness and photocatalysis of crystalline TiO 2 -thin film for self-cleaning application on a photovoltaic covering glass, Mater. Chem. Phys. 289 (2022), 126427, https://doi.org/10.1016/j.matchemphys.2022.126427.
[45] S. Wannapop, A. Somdee, T. Bovornratanaraks, Experimental study of thin film Fe2O3/TiO2 for photocatalytic Rhodamine B degradation, Inorg. Chem. Commun. 128 (2021), 108585, https://doi.org/10.1016/j.inoche.2021.108585.
[46] M. Pérez-González, S.A. Tomás, J. Santoyo-Salazar, S. Gallardo-Hernández, M. M. Tellez-Cruz, O. Solorza-Feria, Sol-gel synthesis of Ag-loaded TiO2-ZnO thin films with enhanced photocatalytic activity, J. Alloys Compd. 779 (2019) 908–917, https://doi.org/10.1016/j.jallcom.2018.11.302.
[47] H. Liu, Y. Hu, Z. Zhang, X. Liu, H. Jia, B. Xu, Synthesis of spherical Ag/ZnO heterostructural composites with excellent photocatalytic activity under visible light and UV irradiation, Appl. Surf. Sci. 355 (2015) 644–652, https://doi.org/10.1016/j.apsusc.2015.07.012.
[48] J. Zhang, J.K. Cha, G. Fu, E.J. Cho, H.S. Kim, S.H. Kim, Aerosol processing of Ag/TiO2 composite nanoparticles for enhanced photocatalytic water treatment under UV and visible light irradiation, Ceram. Int. 48 (2022) 9434–9441, https://doi.org/10.1016/j.ceramint.2021.12.140.
[49] C. Chen, W. Ma, J. Zhao, Semiconductor-mediated photodegradation of pollutants under visible-light irradiation, Chem. Soc. Rev. 39 (2010) 4206–4219, https://doi.org/10.1039/b921692h.